Quantum confinement and ultrafast dephasing dynamics in InP nanocrystals

U. Banin, G. Cerullo, A. A. Guzelian, C. J. Bardeen, and A. P. Alivisatos

Department of Chemistry, University of California, Berkeley, California 94720
and Lawrence Berkeley National Laboratory, 1 Cyclotron Road, Berkeley, California 94720

C. V. Shank

Department of Chemistry, University of California, Berkeley, California 94720;
Department of Physics, University of California, Berkeley, California 94720;
and Lawrence Berkeley National Laboratory, 1 Cyclotron Road, Berkeley, California 94720

The electronic level structure and dephasing dynamics of InP nanocrystals in the strong quantum-confinement regime are studied by two complementary techniques: nanosecond hole burning and the femtosecond three-pulse photon echo. Hole burning yields the homogeneous electronic level structure while the photon echo allows the extraction of the linewidth of the band-gap transition. The congestion of electronic levels observed close to the band-edge transition in the hole-burning experiments gives rise to a pulse-width-limited initial decay in the photon-echo signal. The level structure is calculated and assigned using a model which includes valence-band mixing. The homogeneous linewidth of the band-edge transition is approximately 5 meV at 20 K and is broadened considerably at higher temperatures. The temperature dependence of the linewidth is consistent with an intrinsic dephasing mechanism of coupling to low-frequency acoustic modes mediated by the deformation potential. Quantum-confinement effects in III-V semiconductor InP are compared to those of the prototypical CdSe II-VI semiconductor nanocrystal system. [S0163-1829(97)02111-5]

I. INTRODUCTION

In a solid, the bands of electronic energy levels are continuous, and the electronic spectra are intrinsically diffuse. In the atomic limit, the density of electronic states is discrete and few broadening mechanisms exist, resulting in narrow electronic transitions (1 kHz–100 MHz). In semiconductor nanocrystals, comprised of tens to tens of thousands of atoms, the question of how discrete electronic transitions develop and how the linewidths vary as a function of size is of both theoretical and practical importance.[1,2] In a simple model of quantum confinement, the localization of the optically generated electron-hole pair in a semiconductor nanocrystal arises from a superposition of bulk k states. The principal effects are a shift of the band gap to higher energy in smaller sizes and the development of a discrete electronic structure. Localization is thus accompanied by the concentration of oscillator strength into just a few transitions. Given the large polarizability of nanocrystals, substantial enhancement of the nonlinear susceptibilities is predicted.[2,3]

Semiconductor nanocrystals exhibit the expected shift of the optical spectra to a higher energy, as well as the development of discrete features in the spectra; however, in nanocrystals of CdSe, which have been investigated extensively due to the high sample quality and narrow size distributions,[4,5] homogeneous absorption linewidths of the band-gap transition of several meV have been observed in hole burning[6,7] and in femtosecond photon-echo measurements.[8,9] In addition the linewidth considerably broadens as the size is reduced. This broadening may be due to extrinsic or intrinsic effects. Extrinsic effects would be ultrafast scattering of charges at defects (surface or interior). Intrinsic mechanisms of line broadening arise by coupling to

the vibrations of the nanocrystals (optical, acoustic).[9,10] The electronic structure in such direct gap semiconductor nanocrystals, which was investigated using size selective optical techniques in the frequency domain, exhibits a complex set of electronic transitions which arises from the mixing of multiple valence bands in finite size.[11,12] The successful spectroscopic identification of these transitions in CdSe is a major accomplishment of quantum confinement theory.[12]

Recent advances in synthesis now make it possible to obtain size selected, crystalline, monodisperse nanocrystal samples of the III-V semiconductor InP.[13–15] In this study we present measurements of the homogeneous electronic level structure and linewidths of these samples and compare them to those of the prototypical II-VI nanocrystal system CdSe. Compared to the II-VI semiconductor, the bonds in InP are more covalent, so that the coupling of optical excitations to the vibrations is expected to change in predictable ways. The effective masses, the spin-orbit splitting, the deformation-potential coupling, and other material parameters are significantly different in InP. This leads to predictable changes in linewidths and electronic structure, allowing us to separate the influence of extrinsic, sample-dependent broadening mechanisms and properties from intrinsic ones, and to test models of confinement in quantum dots.

Nanocrystal samples typically exhibit inherent inhomogeneous broadening primarily due to size variations in the ensemble. In addition, a congestion of electronic transitions is possible, as there may be several electronic transitions lying close to the band edge. We use two complementary techniques to study the homogeneous spectroscopy of InP nanocrystals. In the frequency domain, transient ns hole burning (HB) is used to investigate the homogeneous electronic level structure.[6,12] In the time domain we use the femtosecond

three pulse photon echo (3PPE), which provides a direct probe of electronic and vibrational dephasing times.[8,9] Both techniques have been used previously in separate studies to investigate the electronic level structure and linewidth issues in CdSe nanocrystals, however this is the first time, to our knowledge, that simultaneous measurements on the same samples are conducted and used in conjunction to gain a self-consistent picture of the dephasing dynamics in nanocrystals from the fs to the ns timescale.

The paper is organized as follows: In Sec. II experimental details of the sample preparation, the hole-burning setup, and the three-pulse photon-echo experiment are given. In Sec. III, results and discussion for the hole-burning experiment are presented followed by results of the femtosecond three-pulse photon-echo measurements. Both experiments are interpreted using a three-level model for the near band-edge absorption in the nanocrystals. A theoretical assignment of the observed levels is presented and finally the dephasing mechanisms are investigated by conducting a temperature dependence of the echo decay rate. Conclusions are presented in Sec. IV.

II. EXPERIMENT

A. Sample preparation

InP samples have been synthesized using the dehalosylation reaction of $InCl_3$ and $P(Si(CH_3)_3)_3$ in the coordinating solvent trioctylphospine oxide at temperatures between 240 °C and 270 °C as reported by Guzelian *et al.*[14] The solvent provides high-temperature medium for annealing the nanocrystals and also acts to passivate the particle surface limiting growth and imparting solubility to individual particles in a variety of organic solvents. The nanocrystals produced are discrete particles ranging in size between 20 and 60 Å in diameter. Following the initial reaction which produces a wide range of particle sizes, distinct distributions are obtained by using size selective precipitation techniques. Structural characterization shows that the particles are highly crystalline with most consisting of a single, faultless crystalline domain and are spherical to slightly elliptical in shape. Size distributions are approximately ±20%. For the low-temperature spectroscopic investigation, the particles were embedded in a polymer film (poly-vinyl-butyral) with thickness of less than 500 μm and typical optical density of 0.4–0.7 at the inhomogeneous excitonic shoulder.

B. Transient nanosecond hole burning

A dye laser pumped by the second or third harmonic of a Q-switched Nd-Yag laser served as the excitation source for the ns HB experiments. A portion of the second or third harmonic of the Nd-Yag was split off, optically delayed by 20 ns, and used to pump a jet containing a mixture of dyes to provide a broadband probe source from the dye fluorescence. Pump and probe were overlapped on the sample which was placed in a continuous He flow cryostat. Typical pump energies of 50 μJ with a spot size of 1 mm in diameter were used, and the signal was checked to ensure linearity in the pump intensity. The probe pulse was dispersed in a spectrograph, and detected by a gated multichannel detector (intensified CCD or intensified diode array). The gated detec-

tion (5-ns gating time) allowed suppression of the unwanted contribution of pump scattering to the HB signal. The hole-burning signal, corrected for residual pump scatter and sample fluorescence, was obtained by using a sequence controlled by shutters on both pump and probe pulses from the following calculation:

$$-\Delta OD = \frac{I_{wp} - I_p}{I_{np}}, \qquad (1)$$

where I_{wp} is probe signal going through the sample with pump, I_p is the contribution of the pump alone, and I_{np} is probe signal going through the sample without pump.

C. Femtosecond three-pulse photon echo

The femtosecond laser system used for the three-pulse photon-echo experiment has been described in detail previously.[16] Briefly, 60-fs pulses generated by a colliding pulse mode-locked dye laser are amplified in a dye amplifier pumped at 8-kHz by a copper vapor laser (CVL). A broadband continuum is generated by subsequently coupling the pulses into an optical fiber. The spectrally broadened pulses are then amplified by a broadband dye amplifier pumped by a second CVL and compressed using a sequence of gratings and prisms.

For the photon-echo experiments on InP nanocrystals we use a selected portion of the amplified pulse spectrum to match the sample absorption onset [see inset of Fig. 3(b)]. The duration of the resulting pulses, which are close to being transform limited, is 20 fs. The nanocrystal sample was cooled by a closed cycle He cold finger cryostat and the temperature was monitored by two diodes at the cold finger and on the opposite side of the sample holder. The integrated echo signal was detected in the phase matched direction $(-\mathbf{k}_1 + \mathbf{k}_2 + \mathbf{k}_3)$ and was measured with a photomultiplier tube using lock-in detection by chopping one of the beams. All measurements were taken in the perturbative regime, as checked by observing the expected cubic dependence of the echo signal on excitation intensity.
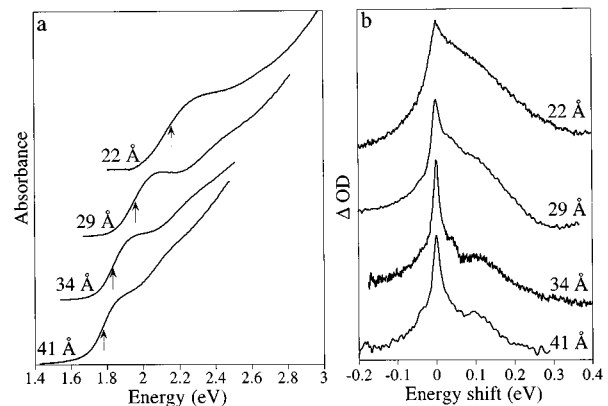
FIG. 1. (a) The absorption spectra ($T=6$ K) for the series of InP nanocrystal samples. Arrows designate the position of the nanosecond excitation pulse for the hole-burning spectra presented in (b).
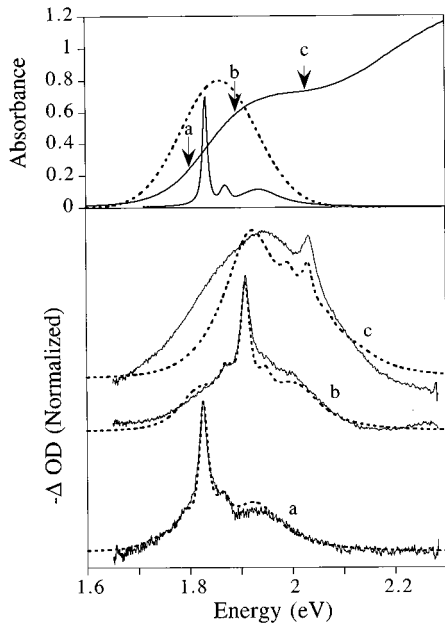
FIG. 2. Nanosecond hole-burning data for the 34-Å InP sample ($T=6$ K). The absorption spectrum is presented in the top frame and the arrows designate the pump energies for the HB experiments shown in the bottom frame. The extracted ''single-particle'' absorption spectrum (solid line) and inhomogeneous distribution (dashed line) are shown in the top frame. The fits obtained using this model are shown as dashed lines in the bottom frame.

III. RESULTS AND DISCUSSION

A. Transient nanosecond hole burning

The low-temperature absorption spectra for a series of InP nanocrystals ranging in size from 22 to 41 Å are presented in Fig. 1(a). Shifts of the absorption edge due to confinement are evident. The spectra are inhomogeneously broadened primarily due to the size distribution and only shoulderlike excitonic features are observed.

Transient ns HB spectra for the series of samples under study are presented in Fig. 1(b). Excitation with a narrow-bandwidth ns laser pulse at the band edge optically selects the largest nanocrystals in the ensemble. The resulting spectral hole enables the extraction of the ''single-particle'' absorption spectra. In all cases, a narrow feature with a size-dependent width ranging from 10 meV for the largest size to 20 meV for the smallest size is accompanied by a broad feature at higher energies.

The homogeneous spectra for the band-edge absorption of these samples can be extracted by conducting an excitation wavelength dependence of the hole-burning spectrum.[6,17] This is presented in Fig. 2, which shows the evolution of the spectral hole with excitation wavelength for the 34-Å InP sample. Upon excitation at the absorption edge, particles are selectively excited at the narrow-band-gap transition leading to a spectral hole that closely resembles the ''single-particle'' absorption spectrum. Aside from a narrow feature at the excitation frequency, a weak phonon side band is observed along with a broad feature spaced at 0.1 eV from the band gap. As the excitation is tuned to the blue, a larger fraction of the distribution is excited into the higher, broadened excited electronic states. The contribution of the narrow
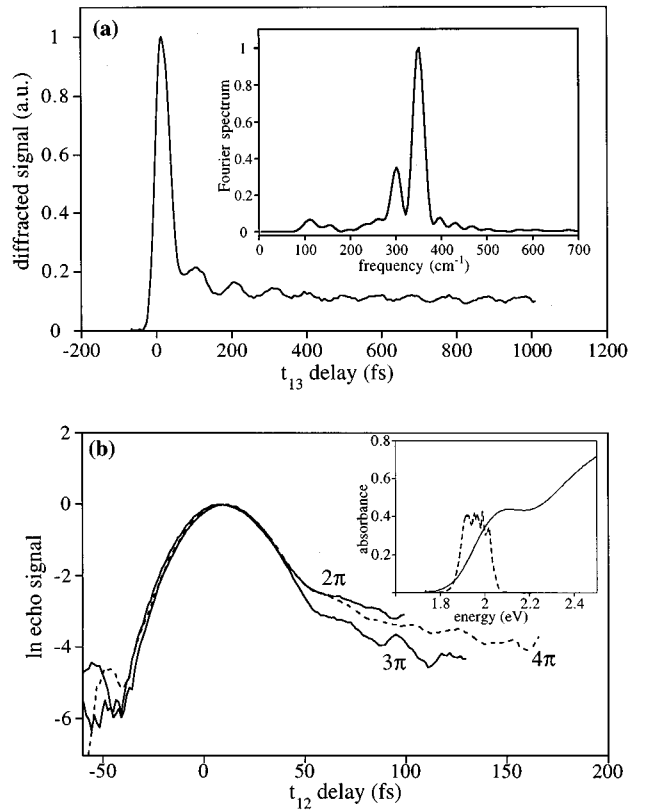
FIG. 3. Three-pulse photon-echo experiments on the 29-Å InP sample ($T=20$ K). (a) Vibrational dynamics measured in the three-pulse photon-echo configuration. The signal as a function of t_{13} with $t_{12}=30$ fs is modulated by optical-phonon modes. The inset shows the Fourier transform of the oscillatory component of the signal. (b) Electronic dephasing measured in the three-pulse photon-echo configuration. Echo decays as a function of t_{12} at three t_{13} delays corresponding to $2\pi/\omega_v$ (solid line), $3\pi/\omega_v$ (solid line), and $4\pi/\omega_v$ (dotted line) conditions are presented. The effect of mode suppression is evident. The inset shows the pulse spectrum (dashed line), along with the low-temperature absorption spectrum.

feature is gradually diminished, appearing as only a small peak above a broad background for the bluest pump frequency [in Fig. 2(c)]. This background reflects the width of the inhomogeneous absorption. The homogeneous absorption and position as well as the width of the inhomogeneous distribution are extracted by fitting the wavelength-dependent hole spectrum. In the limit of linear response to pump energy, far from saturation, we use the following formula:[16,17]

$$-\Delta\text{OD}(v) = C' \int_{-\infty}^{\infty} H(v-v')H(v_{\text{pump}}-v')g(v'-v_0)dv'$$

(2)

where $H(v)$ is the homogeneous ''single nanocrystal'' absorption line shape, $g(v-v_0)$ is the inhomogeneous distribution centered at v_0, and C' is proportional to the excitation intensity.

The ''single-particle'' absorption extracted from the modeling (see Fig. 2) consists of a Lorentzian band-gap transition with a width of 10 ± 2 meV, a phonon side band spaced at

330 cm^{-1} from the band gap, and a second excited transition spaced at 0.10 eV with a width of 0.10 eV. The extracted oscillator strength of the second state is 1.5 times larger than that of the band-gap transition. The inhomogeneous Gaussian distribution has a width of 0.17 eV and is centered at 1.86 eV. We do not include in the model possible induced absorption from the excited state(s), and since we are in the linear regime biexciton effects are neglected.

B. Femtosecond three-pulse photon echo

The width of the band-edge transition extracted from the HB experiments as discussed above is broadened considerably compared with atomic linewidths. The HB measurement takes place on a nanosecond time scale in which various broadening mechanisms not strictly related to the homogeneous linewidth may be active.[18] We thus complement the frequency domain measurements with a direct time domain probe of the electronic dephasing dynamics—the 3PPE which allows the investigation of linewidths and line broadening mechanisms on the fs timescale.[19–21]

In the 3PPE the electronic dephasing can be measured while circumventing the complications arising from coupling to vibrational modes, which leads to modulation of the echo decay by vibronic quantum beats.[8,9,16] A sequence of three pulses is used in this experiment. The first pulse generates a coherent polarization in the material, the second pulse interacts with the polarization forming a population grating, and the third pulse is scattered off the grating in a phase-matched direction. Proper tuning of the third-pulse delay to $2\pi/\omega_v$, where ω_v is the frequency of the coupled vibrational mode, effectively suppresses the contribution of the vibronic quantum beats to the echo decay. The mode suppression is particularly important for systems in which the electronic dephasing is on the order of a vibrational period. In these cases, the two-pulse photon-echo response without mode suppression is strongly modulated by the vibrational beat resulting in an extremely rapid decay which does not accurately reflect the true dephasing of the system.[8,9,16]

The 3PPE experiment was conducted on the 29-Å InP nanocrystal sample, using 20-fs pulses centered at 1.95 eV so as to overlap with the absorption onset [see inset of Fig. 3(b)]. All pulses are linearly polarized with parallel polarization. Two different experiments have been performed to examine in the first case the vibrational dynamics, and in the second case the electronic dephasing.

The vibrational dynamics are studied by setting the first and second pulse at a fixed delay $-t_{12}=30$ fs and detecting the scattered signal as a function of the third-pulse delay t_{13} [Fig. 3(a)]. In this case ($t_{12}>0$, $t_{13}>t_{12}$) a population grating is formed and the signal is modulated by coherent optical-phonon modes. By increasing the fixed delay t_{12} the modulation depth is increased but the overall signal decreases as the polarization dephases in the t_{12} interval. The delay $t_{12}=30$ fs is chosen to yield the best signal to noise ratio for the oscillatory component. The Fourier spectrum of the oscillatory component shows two modes at 350 and 310 cm^{-1} [inset of Fig. 3(a)]. Similar modes are observed in the resonance Raman spectrum of InP nanocrystals.[14] The frequencies of the two modes, assigned to the LO (350 cm^{-1}) and TO (310 cm^{-1}) phonons, correlate well with the phonon

frequencies in bulk InP. Both modes are coupled to the optical transition, while in II-VI nanocrystals only the LO mode is observed.

The electronic dephasing in the 3PPE case is measured by setting t_{13} at a fixed delay to suppress the contribution of LO modes and detecting the scattered signal as a function of t_{12}. Figure 3(b) exhibits the echo signal for three different t_{13} delays corresponding to $t_{13}=2\pi/\omega_v$ (95 fs), $t_{13}=3\pi/\omega_v$ (135 fs), $t_{13}=4\pi/\omega_v$ (190 fs). Data are presented only for delays $t_{12}<t_{13}$. At longer delays, $t_{12}>t_{13}$, the echo signal no longer represents a polarization decay but measures the decay of the excited-state population and cannot be used to extract T_2. In the three cases, the echo signal exhibits a fast pulse-width-limited initial response, followed by a slower decay. As expected, the slow decay is observed to be strongly dependent on the timing of the third-pulse delay (t_{13}) due to the mode suppression. For $t_{13}=2\pi/\omega_v$ the modulation of the signal by the vibrational beat is suppressed, for $t_{13}=3\pi/\omega_v$ the modulation is maximal and a faster decay is observed, finally for $t_{13}=4\pi/\omega_v$, the decay is longer relative to the 3π case as suppression is effective again. This is a manifestation of the effect of quantum beats of the coupled phonon modes on the observed decay and demonstrates the utility of 3PPE in extracting reliable T_2 times when a vibrational mode is coupled to the electronic transition. The t_{13} delays were chosen to suppress the more strongly coupled LO-phonon mode at 350 cm^{-1}. The TO mode is close in frequency and thus is also effectively suppressed.

The magnitude of the LO coupling, quantified by the Huang-Rhys parameter S, can be extracted from a fit to the 2π, 3π, and 4π data.[9] Such a fit yields a value of $S=0.08$ for this sample. This is lower than the value reported for CdSe nanocrystals of similar size ($S=0.18$).[9,22] This can be explained by considering that coupling to LO modes occurs via the Fröhlich mechanism—the electronic excitation alters the charge distribution and distorts the lattice. As expected, the coupling is weaker in the more covalent III-V material, since the Fröhlich mechanism is polar in nature.

An intriguing aspect of the echo response in the electronic dephasing measurement [Fig. 3(b)] is the presence of a pulse-width-limited initial decay. For an inhomogeneously broadened two-level system, a calculation of the echo response for the 3PPE case using real pulses within a third-order perturbation expansion with all terms predicts a *single* exponential decay with a time constant of $T_2/4$ where T_2 is the electronic dephasing time.[20]

C. Interpretation of the echo response

To understand the observed echo response we need to consider the HB spectra for the same sample which show that a two-level system is inadequate to describe the band-edge absorption of the nanocrystals. The HB data for the 29-Å InP sample is presented in Fig. 4(a). As for the 34-Å sample shown in Fig. 2, the HB data shows that above the lowest band-gap transition lies an additional electronic transition.

We model both HB and 3PPE results within this three-level picture (ground state $|a\rangle$ and two excited states $|b\rangle$ and $|c\rangle$ separated by ΔE_{bc}). For HB we repeat the procedure
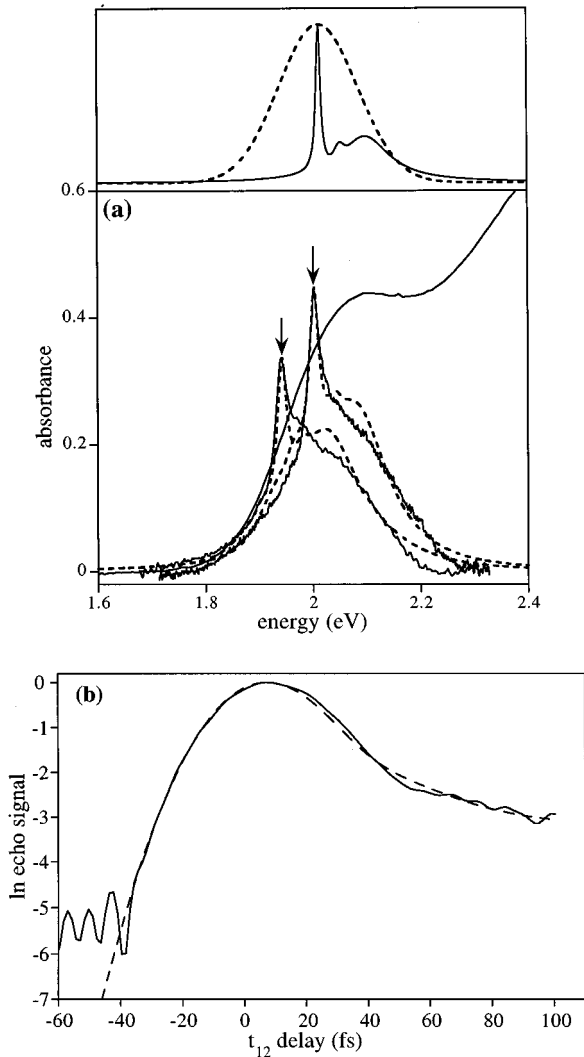
FIG. 4. Simultaneous modeling of HB and 3PPE data for the 29-Å InP sample. (a) HB data (solid lines) and fits (dashed lines). Arrows designate the position of the pump pulse. The top frame shows the extracted ''single-particle'' absorption spectrum (solid line) and inhomogeneous distribution (dashed line) with the following parameters; inhomogeneous distribution: $\Gamma_{in}=0.17$ eV, $E_{in}=2.0$ eV; homogeneous absorption: $\Gamma_{ab}=11$ meV, $\Delta E_{vib}=330$ cm^{-1}, $\Delta E_{bc}=0.09$ eV, $\Gamma_{ac}=0.11$ eV, $\mu_{ca}/\mu_{ba}=1.9$. (b) 3PPE electronic dephasing measurement for the 2π delay (solid line) and model (dashed line). See text for details.

followed for the 34-Å sample and extract a ''single-particle'' absorption spectrum which consists of a band-gap Lorentzian transition ($|a\rangle\rightarrow|b\rangle$, width Γ_{ba}, dipole moment μ_{ba}), a phonon sideband (spacing ΔE_{vib}), and a second broad excited transition ($|a\rangle\rightarrow|c\rangle$, width Γ_{ca}, dipole moment μ_{ca}), [see Fig. 4(a)]. Additional parameters that are included in the model are the linewidth (Γ_{in}) and center (E_{in}) of the inhomogeneous distribution $g(\omega)$ (see caption of Fig. 4 for the exact parameters). The presence of the higher-lying transition in InP nanocrystals is confirmed by theoretical level structure calculation (Sec. III D).

The 3PPE data was modeled using a Bloch equation formalism. The optical Bloch equations[23] were written for the three-level system described above within the rotating wave

and electric dipole approximations. Coupling of the transition to optical phonons, which is effectively suppressed in the experiment by the timing of the third-pulse delay, was excluded. We assume different homogeneous linewidths $\Gamma_{ba}=1/(\pi T_{2ba})$ where T_{2ba} represents a polarization dephasing time for the $|a\rangle\rightarrow|b\rangle$ transition, and $\Gamma_{ca}=1/(\pi T_{2ca})$ were T_{2ca} represents a polarization dephasing time for the $|a\rangle\rightarrow|c\rangle$ transition. Negligible population decay is assumed in the time window of the experiment. The equations were solved within the perturbative approach,[8,9,19] using real pulse widths, to calculate the third-order matrix elements $\rho_{ba}^{(3)}(t,t_{12},t_{13})$ and $\rho_{ca}^{(3)}(t,t_{12},t_{13})$. In the phase-matched direction $-\mathbf{k}_1+\mathbf{k}_2+\mathbf{k}_3$, the radiated polarization is a superposition of the contribution of the two transitions $|a\rangle\rightarrow|b\rangle$ and $|a\rangle\rightarrow|c\rangle$, and the echo response is calculated as the square of this polarization. The fit is presented in Fig. 4(b) as the dashed line. Aside from the linewidth of the band-gap transition (Γ_{ba}), all the parameters used to fit the echo response are identical to those extracted from the fit to the HB data. This analysis provides the following interpretation: the fast pulse-width-limited initial decay in the echo response is associated with the contribution of the excited transition. The slow component of the decay which follows (decay constant$=70\pm10$ fs) yields a T_{2ba} time of 280 ± 40 fs for the band-gap transition. The $|a\rangle\rightarrow|b\rangle$ transition linewidth extracted from this dephasing time is 5 ± 1 meV compared to 11 ± 2 meV extracted from HB. This disparity in linewidth can be explained taking into account the six orders of magnitude difference in the time scales of the two measurements. The HB experimental linewidth is additionally broadened by processes occurring on the ns time scale such as spectral diffusion,[18] and possibly by the presence of an electron and hole pair trapped on the excited nanocrystals which exert an electric field acting to Stark shift and broaden the transition.[24] It should be noted that both the HB and the 3PPE results are also consistent with the broad high-energy transition being composed of a manifold of overlapping states. In this case, the broad excited transition in the model represents the manifold of states.

The appearance of an instantaneous fast decay component in 2PPE experiments has been reported previously in quantum well samples.[25,26] Two primary mechanisms have been shown to contribute to the appearance of the instantaneous response—the first is the interaction induced mechanism which is a many-body effect resulting from coherent exciton-exciton interaction.[25] This mechanism can be ruled out in the present case as coherent exciton-exciton interactions cannot be present since the average distance between the nanocrystals is estimated to be hundreds of angstroms, and in the intensity regime of this study the excitation density is much less than one exciton per nanocrystal. In this respect, the nanocrystal response is analogous to that of a molecule.

The second mechanism, reported by Kim *et al.* who conducted time and spectrally resolved four-wave-mixing experiments on quantum well samples[26] is assigned to the free-induction decay of off-resonant laser fields, which is enhanced by the strong pulse overlap and the resulting population grating near zero delay in the 2PPE case. This mechanism is ruled out in the present study as our experiments are conducted on resonance with no detuning [laser bandwidth smaller than the inhomogeneous absorption width, refer to

inset of Fig. 3(b)] and the off resonance contribution is expected to be minimized. Furthermore, in other systems such as CdSe nanocrystals a similar fast decay was observed to depend systematically on size with diminishing contribution in the smaller nanocrystals.[8,9] Finally, the consistency of the 3PPE and the HB experiments and the ability to model both of them simultaneously within the three-level picture described above provides conclusive evidence for our assignment of the echo response.

This case presents an interesting limit for the four-wave-mixing response in a correlated inhomogeneously broadened three-level system.[27] In the limit of two narrow transitions with similar values of T_2, the short pulse will create an electronic quantum beat. However, for InP nanocrystals the second state homogeneous width is comparable to the energy splitting between the two states and the electronic quantum beat is overdamped. Thus in our measurements we observe a pulse-width-limited initial response arising from the contribution of the second broad transition, followed by a slow decay which arises from the band-gap state. In the following section we will present results of a calculation of the size-dependent level structure in InP nanocrystals consistent with the observed transitions.

Our findings point out the complementary nature of the time domain 3PPE approach and the frequency domain hole-burning measurement in examining the homogeneous optical properties of nanocrystal samples. Hole burning yields the homogeneous electronic level structure. However, the homogeneous linewidth can be extracted only from the more direct fs 3PPE experiment, since on the ns time scale additional broadening mechanisms are present.

D. Assignment of the observed transitions

The zero-order effective-mass approach for the calculation of energy levels in quantum dots takes into account only single valence and conduction bands confined within infinite spherical wells.[28,29] In this case, both hole and electron wave functions are a product of a spherical harmonic and a Bessel function. Simple selection rules of $\Delta n = 0$, $\Delta l = 0$ [n is the electron (hole) level number, l is the electron (hole) orbital angular momentum] are obtained. This zero-order treatment predicts the confinement related blueshift of the gap as well as the appearance of discrete levels. However, while the single-band description is sufficient for the conduction-band states, Efros and co-workers have demonstrated that in the quantum dot regime substantial mixing takes place among the valence-band levels.[11,30] We find that this is also the explanation for the multiple transitions observed at the band edge of the InP nanocrystals. The proper description of the hole levels is obtained by applying spherical boundary conditions onto the Luttinger Hamiltonian. The starting point of the treatment is the usual three-band Luttinger description for the valence bands. After applying the spherical boundary conditions, the only good quantum numbers are the total hole angular momentum $F = L_h + J$ (L_h is the orbital angular momentum of the lowest contributing hole level, J is the total angular momentum before mixing), and the parity. This treatment was previously applied to the II-VI systems, as well as to other quantum dots.[11,12,31] We adopt the notation of Ekimov *et al.*[11] for quantum dot states; hole levels are
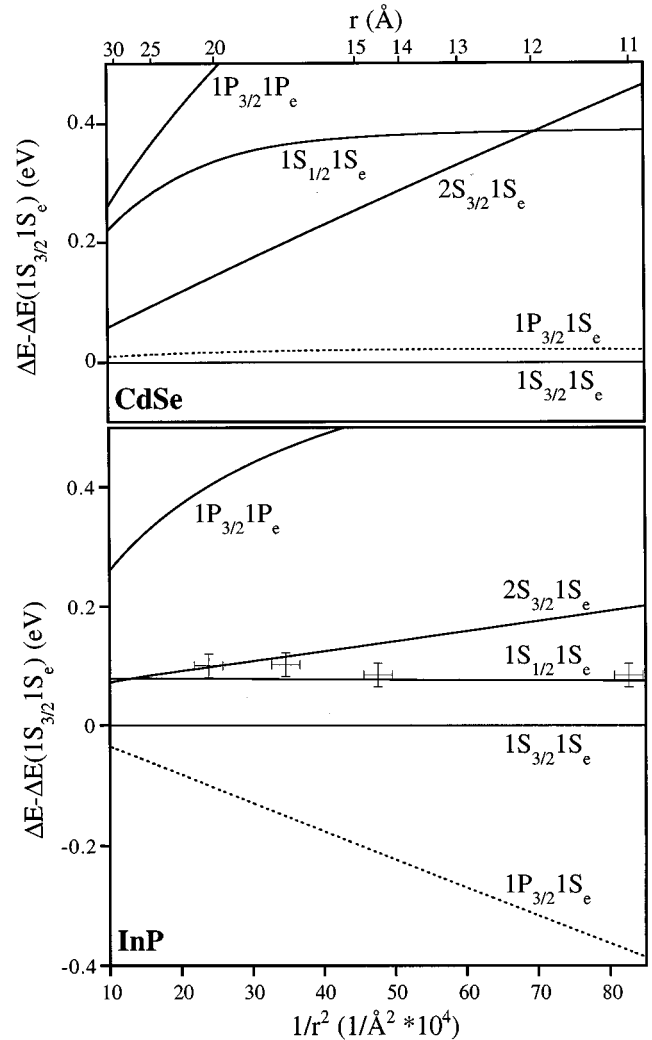
FIG. 5. Calculated excitonic transitions for InP nanocrystals versus size (lower frame). ΔE between the higher-energy transitions and the lowest $1S_{3/2}1S_e$ transition is shown. Crosses designate the measured position of the excited transition as extracted from the HB data in Fig. 1. A similar calculation for CdSe is presented in the top frame for comparison. The $1P_{3/2}$ hole level is shown as a dashed line for both materials. We use bulk literature parameters for both materials (Ref. 34).

designated by nL_F where n is the level number, L represents the orbital angular momentum of the lowest contributing hole sublevel, and F is the total hole angular momentum; electron levels are designated by nl_e where n is the level number and l_e is the orbital angular momentum. The selection rules are then ($L_h - l_e = 0$).

The results of calculation of the size-dependent energies of the first few transitions relative to the band-edge transition between the $1S_{3/2}$ hole and the $1S_e$ electron levels are presented in Fig. 5 for InP and CdSe for comparison. The relative positions of the second excited state extracted from the HB spectra for the InP samples shown in Fig. 1(b) is marked by crosses on Fig. 5 (bottom frame). This allows us to assign the observed transitions; the lowest excitonic transition is between the $1S_{3/2}$ hole level and the $1S_e$ electron level. Two transitions are energetically consistent with the second excited state; $2S_{3/2}1S_e$ and $1S_{1/2}1S_e$.
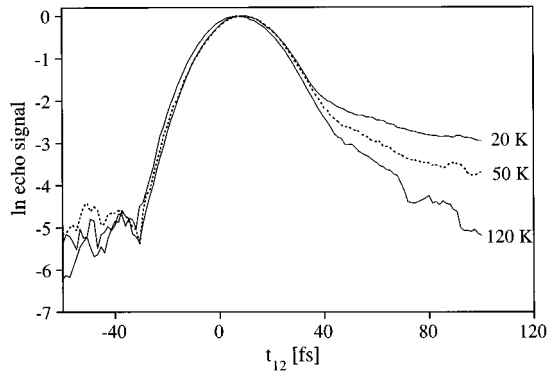
FIG. 6. Electronic dephasing measurements in the 3PPE configuration ($t_{13}=95$ fs, $2\pi/\omega_v$ conditions) for the 29-Å InP sample at three temperatures.

FIG. 7. Temperature dependence of the echo decay rate for 29-Å InP (circles) and CdSe nanocrystals (crosses). The solid lines are the simulated decay rates for the model described in the text.

A comparison of the level structure of InP with CdSe reveals that the small value of the spin-obit splitting Δ in InP leads to a congestion of electronic transitions close to the band-gap. The transitions do not fan out with size as reported for CdSe; in fact, in InP nanocrystals the energy of the $1S_{1/2}1S_e$ transition gradually gets closer to the band-gap as the size is reduced. An additional difference in the predicted level structure of InP and CdSe is in the ordering of the lowest hole levels. In CdSe the lowest hole level is $1S_{3/2}$ and the second hole level $1P_{3/2}$ always lies energetically higher [see Fig. 5(b), dashed line]. In InP, however, the $1P_{3/2}$ hole level is energetically lower than the $1S_{3/2}$ level. Although this is not expected to affect the absorption of the nanocrystals (the $1P_{3/2}1S_e$ level is optically dark), it may have an effect on the luminescence properties of InP, as the hole can float up to the $1P_{3/2}$ level affecting the radiative recombination of electron and hole.

E. Line-broadening mechanisms

An issue of considerable importance is to examine the various contributions to the homogeneous linewidth of the lowest transition in the nanocrystals. One wishes to assess whether the observed width is an intrinsic size effect or whether it is an extrinsic effect of scattering from surface or interior defects which may be defeated by improved sample preparation. The nature of the dephasing mechanisms can be investigated by conducting a temperature dependence of the linewidth. The 3PPE data for three temperatures for the 29-Å InP nanocrystal sample are presented in Fig. 6. Shown are electronic dephasing measurements of the echo response as a function of t_{12} with t_{13} set at the fixed delay of $2\pi/\omega_v$. The slow decay component assigned to the band-gap transition is clearly becoming faster as temperature is increased. Linear fits to the slow component in the 3PPE case allows us to extract the temperature dependence of the linewidth of the band-gap transition. The extracted decay rates for the slow component are shown in Fig. 7. Multiple points from several separate sets of measurements are presented, along with the echo decay rate for a CdSe sample of the same size reported by Mittleman *et al.* in an earlier work (see Ref. 9 and references therein for experimental details). Compared with CdSe
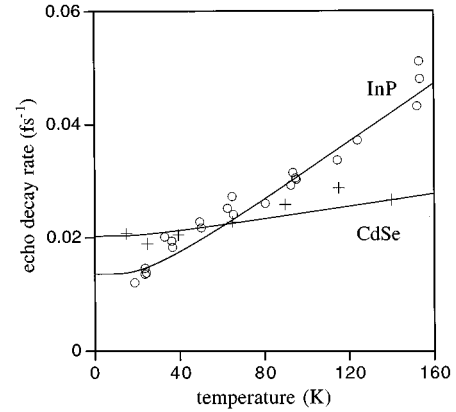
nanocrystals, the low-temperature dephasing rate is slower in InP, but the slope of the temperature dependence is considerably steeper.

An intrinsic dephasing mechanism which is consistent with the temperature dependence of the dephasing rate for both materials is the coupling to low-frequency acoustic modes which serve as a heat bath.[10,32] Such coupling is mediated by the deformation potential. The coupling strength, g_a, to a mode of frequency ω_a can be extracted from the following formula:[6]

$$g_a \approx \frac{(D_e - D_h)^2}{\pi r^3 C_{11} \hbar \omega_a}, \qquad (3)$$

where $(D_e - D_h)$ is the deformation potential for the bulk material,[33] C_{11} is the bulk elastic modulus,[34] and r is the nanocrystal radius. Using this formula and the material parameters for InP and CdSe, the temperature dependence of the echo decay rate in both cases is reproduced (Fig. 7, solid lines). The only free parameter is an offset which represents the temperature-independent contribution to the echo decay rate resulting from elastic scattering at surface or interior defects (0.0044 fs^{-1} in InP, 0.018 fs^{-1} in CdSe). The larger deformation-potential coupling (1.0 versus 0.4 for InP and CdSe, respectively) and higher average acoustic frequencies calculated for modes of an elastic 29-Å sphere[35] in InP with respect to CdSe lead to a considerably steeper temperature dependence for InP nanocrystals. In our measurements we do not access the temperature regime in which broadening due to LO phonons is expected to contribute due to pulse width and S/N limitations[8] (the LO-phonon frequency in InP is 350 cm^{-1} and the mode will not be significantly thermally populated at $T=150$ K).

The intrinsic acoustic-phonon-coupling mechanism accounts for most of the observed zero-temperature linewidth of the InP sample. Negligible in the bulk, the deformation-potential coupling strength is enhanced with decreasing size. This arises from the enhanced deformation, averaged over fewer bonds, induced by the transition of the electron from a bonding to an antibonding orbital. The average acoustic bath frequencies are also larger for smaller sizes. The overall effect is considerable broadening at small diameters, which is

qualitatively observed in the hole-burning spectra for the series of samples shown in Fig. 1(b).

The deformation-potential coupling mechanism predicts a $1/r^5$ dependence of the linewidth on size. This suggests that while in the very small sizes considerable intrinsic broadening is present, there is a size regime in which the simple confinement pictures suffice and the spacing of the electronic transitions greatly exceeds the linewidth. This size regime is material dependent. In InP nanocrystals with a radius of 50 Å, the predicted intrinsic low-temperature linewidth is 0.002 meV, and even at 300 K the linewidth is predicted to broaden only to 0.06 meV by this particular mechanism.

IV. CONCLUSIONS

InP nanocrystals in the size range below 50-Å in diameter exhibit an electronic structure of a band-edge transition along with close-lying excited states, assigned within a model of a particle in a spherical box including the effects of valence-band mixing. The excited transitions, as observed by ns hole burning, are broadened and congested leading to a pulse-limited fast decay component in the fs 3PPE measurements. The band-gap transitions have linewidths on the order of a few meV. Direct 3PPE measurements for 29-Å samples show that the low-temperature electronic dephasing time is 280 ± 40 fs. The temperature dependence is consistent with a line-broadening mechanism which results from coupling to low-frequency acoustic modes. This intrinsic mechanism limits the linewidth in highly confined quantum dots.

Compared to the CdSe nanocrystal system, we find that the Fröhlich coupling to LO phonons is smaller in InP. The TO mode is also coupled to the electronic transition unlike the more polar CdSe case. The observed and calculated level structure is found to be more congested in InP primarily because of the smaller spin-orbit splitting in the bulk. The low-temperature linewidth for 29-Å InP is smaller than that observed for similar size CdSe, but the temperature dependence of the broadening is considerably steeper indicating stronger deformation-potential mediated coupling to acoustic phonons in InP nanocrystals.

*Permanent address: Dipartimento di Fisica del Politecnico, Piazza L. Da Vinci 32, 20133 Milano, Italy.

[1] A. P. Alivisatos, Science **271**, 933 (1996).

[2] L. E. Brus, Appl. Phys. A **53**, 465 (1991).

[3] S. Schmitt-Rink, D. A. B. Miller, and D. S. Chemla, Phys. Rev. B **35**, 8813 (1987).

[4] C. B. Murray, D. J. Norris, and M. G. Bawendi, J. Am. Chem. Soc. **115**, 8706 (1993).

[5] J. E. Bowen Katari, V. L. Colvin, and A. P. Alivisatos, J. Phys. Chem. **98**, 4109 (1994).

[6] A. P. Alivisatos, A. L. Harris, N. J. Levinos, M. L. Steigerwald, and L. E. Brus, J. Chem. Phys. **89**, 4001 (1988).

[7] M. G. Bawendi, W. L. Wilson, L. Rothberg, P. J. Carrol, T. M. Jedju, M. L. Steigerwald, and L. E. Brus, Phys. Rev. Lett. **65**, 1623 (1990).

[8] R. W. Schoenlein, D. M. Mittleman, J. J. Shiang, A. P. Alivisatos, and C. V. Shank, Phys. Rev. Lett. **70**, 1014 (1993).

[9] D. M. Mittleman, R. W. Scshoenlein, J. J. Shiang, V. L. Colvin, A. P. Alivisatos, and C. V. Shank, Phys. Rev. B **49**, 14 435 (1994).

[10] T. Takagahara, Phys. Rev. Lett. **71**, 3577 (1993).

[11] A. I. Ekimov, F. Hache, M. C. Schanne-Klein, D. Ricard, C. Flytzanis, I. A. Kudryavtsev, T. V. Yazeva, A. V. Rodina, and A. L. Efros, J. Opt. Soc. Am. B **10**, 100 (1993).

[12] D. J. Norris, A. Sacra, C. B. Murray, and M. G. Bawendi, Phys. Rev. Lett. **72**, 2612 (1994); D. J. Norris and M. G. Bawendi, Phys. Rev. B **53**, 16 338 (1996).

[13] O. I. Micic, C. J. Curtis, K. M. Jones, J. R. Sprague, and A. J. Nozik, J. Phys. Chem. **98**, 4966 (1994); O. I. Micic, J. R. Sprague, C. J. Curtis, K. M. Jones, J. L. Machol, A. J. Nozik, H. Geissen, B. Fluegel, G. Mobs, and N. Peyghambarian, *ibid.* **99**, 7754 (1995).

[14] A. A. Guzelian, J. E. B. Katari, A. V. Kadavanich, U. Banin, K. Hamad, E. Juban, A. P. Alivisatos, R. H. Wolters, C. C. Arnold,

and J. R. Heath, J. Phys. Chem. **100**, 7212 (1996).

[15] H. Geissen, B. Fluegel, G. Mohs, N. Peyghambarian, J. R. Sprague, O. I. Macic, and A. J. Nozik, Appl. Phys. Lett. **68**, 304 (1996).

[16] C. J. Bardeen and C. V. Shank, Chem. Phys. Lett. **203**, 535 (1993).

[17] D. J. Norris and M. G. Bawendi, J. Chem. Phys. **103**, 5260 (1995).

[18] D. W. Peck, L. R. Narasimhan, and M. D. Fayer, J. Chem. Phys. **92**, 4125 (1990).

[19] S. Mukamel, in *Principles of Nonlinear Optical Spectroscopy* (Oxford, New York, 1995).

[20] A. M. Weiner, S. De Silvestri, and E. P. Ippen, J. Opt. Soc. Am. B **2**, 645 (1985).

[21] C. Bardeen, G. Cerullo, and C. V. Shank, in *Ultrafast Phenomena X*, edited by P. F. Barbara, W. H. Knox, J. Fujimoto, and W. Zinth (Springer-Verlag, Berlin, 1996), p. 197.

[22] J. J. Shiang, Ph.D. thesis, University of California, Berkeley, California, 1995.

[23] N. Bloembergen, in *Nonlinear Optics* (Benjamin, New York, 1965).

[24] Y. Wang, A. Suna, J. McHugh, E. F. Hilinski, P. A. Lucas, and R. D. Johnson, J. Chem. Phys. **93**, 6927 (1990).

[25] D. S. Kim, J. Shah, T. C. Damen, W. Schafer, F. Jahnke, S. Schmitt-Rink, and K. Kohler, Phys. Rev. Lett. **69**, 2725 (1992).

[26] D. S. Kim, J. Shah, T. C. Damen, W. Schafer, L. N. Pfeiffer, and K. Kohler, Phys. Rev. B **50**, 15 086 (1994).

[27] M. Kock, J. Feldmann, E. O. Goebel, P. Thomas, J. Shah, and K. Koehler, Phys. Rev. B **48**, 11 480 (1993).

[28] Al. L. Efros and A. L. Efros, Fiz. Tekh. Poluyprovodn. **16**, 1209 (1982) [Sov. Phys. Semicond. **16**, 772 (1982)].

[29] L. E. Brus, J. Chem. Phys. **80**, 4403 (1984).

[30] G. B. Grigoryan, E. M. Kazaryan, Al. L. Efros, and T. V. Yazeva,

Fz. Tverd. Tela (Leningrad) **32**, 1772 (1990) [Sov. Phys. Solid State **32**, 1031 (1990)].

[31] T. Richard, P. Lefebvre, H. Mathieu, and J. Allegre, Phys. Rev. B **53**, 7287 (1996).

[32] S. Nomura and T. Kobayashi, Solid State Commun. **82**, 335 (1992).

[33] A. Blacha, H. Presting, and M. Cardona, Phys. Status Solidi B **126**, 11 (1984).

[34] *Physics of Group IV Elements and III-V Compounds*, edited by K. H. Hellwege, Landolt-Börnstein, New Series, Group III, Vol. 17, Pt. a (Springer-Verlag, Berlin, 1982), pp. 281–297.

[35] H. Lamb, Proc. London Math. Soc. **13**, 189 (1982).